Kinetic Monte Carlo simulations of the water gas shift reaction on Cu(111) from density functional theory based calculations

Hèctor Prats, Leny Álvarez, Francesc Illas and Ramón Sayós*

Departament de Química Física and Institut de Química Teòrica i Computacional (IQTCUB), Universitat de Barcelona, C. Martí i Franquès 1, 08028 Barcelona, Spain

ABSTRACT

A systematic first-principles kinetic Monte Carlo study of the water gas shift reaction taking place on the Cu(111) surface is presented including adsorption/desorption, diffusion and other elementary chemical reactions, totalling 34 elementary steps with all reaction rates obtained from periodic density functional theory based calculations. The kinetic Monte Carlo simulations were carried out at different partial pressures and temperatures. The results show that the diffusion processes cannot be neglected and that the reaction proceeds predominantly through an associative mechanism via a carboxyl intermediate. The analysis of temperature dependence shows an Arrhenius behaviour with an apparent activation energy of 0.5-0.8 eV in agreement with experiments and with previous microkinetic studies. The effect of H_2O/CO ratio on this reaction shows that mixtures with higher CO proportion enhance the reactivity, also in accordance to previous studies. The present work allows one to ascertain the relative importance of the different steps in the mechanism of water gas shift reaction over Cu(111) at several conditions as well as to see the coverage evolution of the surface.

KEYWORDS: Kinetic Monte Carlo, water gas shift reaction, density functional theory, mechanisms, redox, associative, carboxyl, copper (111) surface, microkinetic model, simulations

* Corresponding author.

E-mail address: r.sayos@ub.edu (R. Sayós)

1. Introduction

The water gas shift reaction (WGSR) involves CO and H_2O to produce CO_2 and H_2. It is an exothermic reaction

$$CO + H_2O \rightarrow CO_2 + H_2, \ \Delta_r H^0_{298.15K} = -0.43 \text{ eV}$$

constituting an important industrial process involved in the production of high purity hydrogen [1]. Hence, this at first sight simple reaction is relevant to the synthesis of ammonia and methanol. It is also involved in the town gas purification and in other important industrial and technologically relevant processes. The interest in the WGSR has been renewed due to the stringent requirements of high purity hydrogen needed in fuel cells [2], where CO concentration below 0.5% is needed to prevent poisoning of the Pt anode, a key component of these devices. Industrially, the WGSR is typically carried out in two stages: a first one at quite high temperature (300°- 450° C) and second one at a lower temperature (200°- 300° C). The high temperature stage uses an iron oxide – chromium oxide based catalysts ($Fe_2O_3/Cr_2O_3/MgO$) [3] while copper based catalysts with inclusion of Zn, Cr and Al oxides [4] and $CuO/ZnO/Al_2O_3$) [5] are used in low temperature reactors [6]. Nevertheless, it is worth pointing out that these catalysts usually require lengthy and quite complex activation steps before usage.

Several alternatives are being investigated to find WGSR catalysts that are active at relatively low temperatures. To this end several theoretical and experimental studies have been undertaken aimed at disclosing the molecular mechanism and thus obtaining the necessary knowledge for potential improvement through a rational design. Two main reaction mechanisms, redox and associative, have been proposed for different catalytic surfaces. The two mechanisms start from H_2O dissociation, but the former continues with OH dissociation to produce adsorbed O atoms whereas in the latter CO_2 is produced through a carboxyl (COOH) intermediate. Among the different types of systems that have been explored one can highlight those involving well-defined metallic surfaces Pd(111) [7], Pt(111) [7,8], Pt(211) [8], Pt(322) [8], Cu(321) [9], Cu(111) [10,11], inverse catalysts constituted by metal oxide nanoparticles supported on metals CeO_x/Cu(111), CeO_x/Au(111) [12], metallic nanoparticles supported on oxides Cu/ZnO $(000\bar{1})$ [13], $Cu/TiO_2(110)$ and $Au/TiO_2(110)$ [14] or, more recently carbides as in the novel Au/TiC(001) system [15]. A series of systems based on other supported gold nanocatalysts have

recently been reviewed [16]. Based on the information extracted from experiments on model catalysts and on theoretical models, more complex systems have been proposed involving a metallic nanoparticle supported on CeO_x nanoparticles which, in turn, are supported in $TiO_2(110)$ [17]. The resulting catalysts have been proven to significantly increase the H_2 production rate [18].

Nevertheless, in spite of the progress in the search of more efficient WGSR catalysts, Cu continues to be at present the main ingredient of the industrially used catalysts. Not surprisingly a huge effort has been devoted to understand the microscopic molecular mechanism of the WGSR catalysed by Cu containing systems. The work of Hadden et al. [19] presented evidence that the activity of the $CuO/ZnO/A1_2O_3$ catalysts on the WGSR can be closely correlated to the copper surface area. Since in this catalysts large Cu particles are present, predominantly exhibiting (111) facets, the Cu(111) surface has been usually taken as a typical benchmark for WGSR studies. In particular, previous studies used Density Functional Theory (DFT) calculations to investigate the WGSR mechanisms on Cu(111) surface, determining the energy barriers of all elementary processes [10, 11] and showing that the associative mechanism via carboxyl species dominates over the redox mechanism via the oxidation of CO by atomic O. This picture was also confirmed by a microkinetic model including in all 32 elementary processes with transition state theory derived reaction rate constants at a temperature of 463 K and pressure of 1 bar, using DFT energy barriers and partition functions [10]. The microkinetic analysis carried out by Gokhale et al. [10] showed as well that water dissociation was the rate-limiting step for WGSR on Cu(111). Nevertheless, in this microkinetic model some reaction rates parameters had to be modified to better match the WGSR experimental data.

In order to reach a more detailed picture beyond the mean field approximation inherent to the microkinetic approach, we present a comprehensive first-principles kinetic Monte Carlo (kMC) study of the WGSR over Cu(111) surface and we analyse the results obtained from kMC simulations at several temperatures and partial pressures. A total of 34 elementary processes are considered, including also CO, OH, H and O surface diffusion processes. Reaction rates for all processes are obtained from DFT data along with transition state theory or collision theory. Some additional DFT calculations were also carried out to complete data missing in the literature. The results of the present kMC study are compared to those from the microkinetic model above mentioned and to other available experimental and theoretical studies.

The rest of paper is organized as follows. Section II includes the description of the lattice-gas model chosen and outlines the set of elementary processes taken into account, it also reports the details of the kMC method and contains important details about the calculation of the different reaction rates, which represents the key ingredient of the whole approach. Section III presents the kMC simulations for several temperatures and partial pressures discussing their effect on the WGSR mechanism and H_2 production. Finally, Section IV summarizes the main conclusions of the present investigation.

2. Theory

2.1 Lattice-gas model

In order to carry out the kinetic Monte Carlo simulations, a suitable model of the surface of interest is needed. In the present work, the Cu(111) surface is represented by a two-dimensional hexagonal periodic grid of L×L points, where each point represents one catalytically active (111) surface site. The convergence with the lattice size has been tested by computing the final (i.e., steady-state) H_2 production for several surface models with different L numbers (i.e., 8-64), concluding that the results for the 25×25 lattice model virtually coincide with those obtained using larger surface models. Periodic boundary conditions have been applied to provide an adequate representation of the periodicity exhibited by the Cu(111) surface. In this way, surface species jumping across the boundary reappear at the opposite side of the lattice. All sites are considered equally probable for adsorption of both reactants species (i.e., CO and H_2O) and it is assumed that an adsorbed species in a given site can interact with its six nearest neighbours in the hexagonal periodic grid. Moreover, all other possible intermediates adsorbed species (e.g., OH, H, COOH,..) will use only one adsorption site, excepting the bidentate formate (HCOO) that needs two sites, as previous DFT calculations have shown [10].

For the present kMC simulations the initial state corresponded to an experiment with a fresh reactants mixture of CO and H_2O with P_{CO} and P_{H2O} partial pressures, continuously impinging on an empty thermalized Cu(111) surface, where the heterogeneous reaction takes place and afterwards the final gas products (i.e., CO_2 and H_2) leave the surface region (i.e., in a nonequilibrium thermodynamic state). A total of 34 elementary processes were considered for

the molecular mechanism of the WGSR, which are described in Table 1. These include all elemental steps considered in a previous microkinetic study of this reaction [10] but with some important refinements in the calculation of the reaction rates as explained in detail below. Thus, the overall mechanism includes adsorption and desorption of reactants (steps ±1 and ±3, where + stands for forward and – for backward for all elementary steps in Table 1), desorption of products (steps –2 and –4) and several surface reactions (steps ±5 to ±16). In addition, four processes involving diffusion of CO, OH, H and O adsorbed species have been considered (steps 17 to 20) because these are the most mobile adsorbates and because were also considered in a previous and similar kMC study of the WGSR on a Cu/ZnO supported model catalyst [13].

2.2 Kinetic Monte Carlo

The kMC method has been used to numerically solve the master equation (ME) by generating an ensemble of trajectories, usually referred to as Poisson processes. ME is the starting point for a stochastic description of the system [20]:

$$\frac{dP_\alpha}{dt} = \sum_\beta \left[W_{\beta\alpha} P_{\beta -} W_{\alpha\beta} P_\alpha \right] \quad (1)$$

where the summation runs over all possible configurations, P_α is the probability that the system is in a α configuration at time t, and $W_{\alpha\beta}$ is the transition probability per unit time that the system will undergo the $\alpha \rightarrow \beta$ configuration transition due to reactions and other processes. This is a lost-gain equation, which can be derived from first-principles. In the kMC procedure, each generated trajectory propagates the system correctly from configuration to configuration in such a way that the average over the entire ensemble of trajectories yields probability density functions for all states fulfilling the ME. A C^{++} code has been written to solve the ME by means of the most widely used rejection-free algorithm, which leads to the so-called direct kMC method [21,22], a type of the variable step size procedure [20].

Once the list of all possible elementary processes on the different lattice sites is obtained, the transition probability (W) of the i^{th} process at j^{th} site (i.e., r_{ij} rate) is calculated and normalized to the total rate r_{tot}

$$\frac{r_{ij}}{\sum_{i=1}^{N_p} \sum_{j=1}^{N_L} r_{ij}} = \frac{r_{ij}}{r_{tot}} \quad (2)$$

where N_P stands for the total number of processes that can occur at the j^{th} site and N_L corresponds to the total number of sites. Then, a (I,J) pair process of the list is selected, proportionally to its relative rate, when fulfils the following condition,

$$\frac{\sum_{i=1}^{I-1}\sum_{j=1}^{J} r_{ij}}{r_{tot}} < \rho \leq \frac{\sum_{i=1}^{I}\sum_{j=1}^{J} r_{ij}}{r_{tot}} \quad (3)$$

ρ is a random number generated from a uniform distribution on the unit interval ($\rho \in [0,1]$) at each step of the simulation. Obviously, a process with a large rate will have a higher chance of being chosen in this way, and this probability-weighted selection is precisely provided by the partial sums in eq. 3. By executing the selected process the system is moved to a new configuration, and the time is advanced by

$$t \rightarrow t + \frac{1}{r_{tot}} \quad (4)$$

Next, the code computes all the new r_{ij} and r_{tot} values and repeats the previous steps until a sufficiently large number of steps have been considered. This typically involves hundreds of millions and is high enough to ensure that the system achieves a steady-state.

The correctness and performance of the present code has been validated by comparing several simulations with those obtained using ZACROS 1.0.1 package, a first-reaction kMC software developed by Stamatakis et al. [23, 24]; for instance, calculating the logarithm of the number of H_2 or CO_2 products formed per site and second (hereafter referred to as turnover frequency, TOF) for T = 625K and partial pressures of CO and H_2O of 26 and 10 Torr (i.e., 34.7 and 13.3 mbar), respectively. The present algorithm predicts a TOF of $10^{3.89}$ s^{-1} whereas ZACROS prediction is of $10^{3.92}$ s^{-1}. The two results are sufficiently close to claim good agreement. Moreover, differences in calculated surface coverage of several adsorbed species using both codes were also checked, showing only a small increase in the OH coverage, going from ~0.20 in our code to ~0.22 in ZACROS; also a very small decrease in the H coverage from ~0.12 to ~0.10 was observed, respectively. The surface coverage for other species was almost the same. The main reason for having developed the present code is to allow for a considerable saving of computational time with respect to ZACROS, which also includes many options, which are not used here.

2.3 Reaction rates

The rate of a surface elementary process, defined as the number of times this process occurs per site and time unit, can be calculated by using either the transition state theory (TST) or the collision theory (CT) [20, 25]. Usually, TST values from DFT results constitute a better choice. For a surface Langmuir-Hinshelwood type reaction or an atomic or molecular diffusion, this rate can be calculated as

$$r_i \equiv r_{ij} = \frac{k_b T}{h} \frac{Q_i^{\neq}}{Q_R} e^{\frac{-\Delta E_i^{0\neq}}{k_b T}} \quad (5)$$

where h denotes Planck's constant, k_b the Boltzmann's constant, and $Q_i^{\neq}$ and Q_R are partition functions (dimensionless) of the transition state and the reactants, respectively. $\Delta E_i^{0\neq}$ stands for the energy barrier for the i^{th} process, including the zero-point energy (ZPE) correction. Moreover, r_i should be multiplied by a statistical factor $l^{\neq}$ (sometimes ignored), which accounts for the several equivalent ways to achieve the transition state, as it is explained in standard kinetic textbooks [25]. In fact, this factor was 2 (default value $l^{\neq}=1$) only for reactions 5, 7 and -8, shown in Table 1. It is also worth pointing out that in microkinetic studies, where classical kinetics differential equations are written for all the elementary steps and numerically integrated (see for instance Ref. 10 and references therein) a similar expression to eq. 5 is used for the rate constant calculation, but including also as a factor the area of the adsorption site (e.g., units for LH rate constants: $m^2\,s^{-1}$).

The rate of adsorption processes of a gas with species of mass m_i at a given temperature T and partial pressure p_i can be calculated from the flux of incident species through the well-known Hertz-Knudsen equation as

$$r_i^{ad} = S_{0,i} \cdot A_{site} \frac{p_i}{\sqrt{2\pi m_i k_b T}} \quad (6)$$

where at a given temperature $S_{0,i}$ stands for the initial sticking coefficient and A_{site} corresponds to the area of a single site. Rigorously speaking, $S_{0,i}$ is introduced to take into account the fact that only a fraction of the incoming molecules will be adsorbed. Nevertheless, in the present study $S_{0,i}$ is taken as the unity for both gas reactants CO [26] and H_2O [27] as in previous studies. A_{site} was calculated always as the total area divided by the number of sites. For Cu, the calculated DFT/PW91 bulk lattice parameter is 3.66 Å [10] (exp. 3.62 Å [28]), and the corresponding

surface unit cell parameter for (111) face turns out to be 2.59 Å, which implies an A_{site} value of 5.80 Å^2.

The rate of desorption processes (i.e., r_i^{des} for i=-1, -3 and -4) can be determined from TST assuming an early 2D gas-like transition state [23] or simply by applying the microscopic reversibility and detailed balance principles [25, 29], although the two approaches produce identical values. The first method implies the use of eq. 5 with

$$\frac{Q_i^{\neq}}{Q_R} = \frac{Q_{vib}^{gas} \cdot Q_{rot}^{gas} \cdot Q_{tras,2D}^{gas}}{Q_{vib}^{ad}} \quad (7)$$

$$Q_{tras,2D}^{gas} = A_{site} \frac{2\pi m_X k_b T}{h^2} \quad (8)$$

The effect of repulsive lateral interactions for CO on Cu(111) on WGSR [13] has been previously included by correcting their desorption energy barriers through the equation

$$\Delta E_{i,lat}^{0\neq} = \Delta E_i^{0\neq} + n\,\Delta E_{lat} \quad (9)$$

where *n* indicates the number of nearest neighbours CO adsorbed molecules and ΔE_{lat} = -0.15 eV. Nevertheless, their effect in the present work was negligible, due to the low CO surface coverage observed (see next section).

For the diffusion processes 17, 18, 19 and 20 (see Table 1), the rate was calculated assuming a typical constant pre-exponential factor of 10^{13} s^{-1} [20], its corresponding DFT calculated energy barrier [13] and a scaling factor ($0 \leq \alpha \leq 1$), which decreases the diffusion to reduce the computational cost but without affecting the results of the simulations [13], as it will be clearly shown in the next section. Hence, diffusion rates were obtained as

$$r_i^{dif} = \alpha \cdot 10^{13}(s^{-1})\, e^{\frac{-\Delta E_{i,dif}^{0\neq}}{k_b T}} \quad (10)$$

Finally, it is necessary to point out that since some of the elementary processes involve hydrogen atom transfer, one needs to introduce a one-dimensional tunnelling correction factor ($\kappa \geq 1$) in the calculation of reaction rates of these processes (i.e., steps ±5, ±6 , ±11 , ±13 and 19, Table 1). The tunnelling correction factor is computed from the expression derived from a symmetrical Eckart barrier [30] as

$$\kappa(T) = 1 + \frac{1}{24}\left|\frac{h\nu_{img}}{k_b T}\right|^2 \left(1 + \frac{k_b T}{\Delta E_i^{0\neq}}\right) \quad (11)$$

where ν_{img} is the imaginary frequency of the transition state. In spite of the fact that the observed effect was very small, all the calculated rates of the above mentioned processes include this correction.

All rates used in the present kMC simulations were calculated from first-principles using available DFT data [10, 13] and the set of equations outlined above. It is important to point out that the ZPE-corrected energy barriers for the exothermic reactions were taken from a previous microkinetics study of the WGSR on Cu(111) [10]. However, for the endothermic ones the ZPE-correction was missing. Thus, harmonic vibrational frequencies to be used both in these missing ZPE-corrected energy barriers and also in the necessary vibrational partition functions were determined from pertinent DFT calculations. Therefore, additional DFT calculations on some gas phase species (i.e., $H_2O_{(g)}$, $CO_{2(g)}$, $OH_{(g)}$, $CO_{(g)}$, $H_{2(g)}$, *trans*-$COOH_{(g)}$ and *cis*-$COOH_{(g)}$) and on several adsorbed species were performed by means of VASP code [31, 32, 33]. A four-layer Cu relaxed slab, periodically repeated in a 2 x 2 supercell with 20 Å of vacuum between any two successive metal slabs was used to model Cu(111). The valence electron density was expanded in a plane-wave basis set with a cut-off of 415 eV for the kinetic energy. The effect of core electrons in the valence electron density was taken into account through the projector augmented wave method [34] as implemented in VASP [35]. The surface Brillouin zone was sampled with a 5 × 5 × 1 Monkhorst-Pack grid of special k-points [36] and the exchange-correlation energy and potential were described by the generalized gradient approximation (GGA-PW91) [37], using the same functional as in previous study [10].

To facilitate the comparison of the different competitive processes, Table 1 summarizes all reaction rates at T = 625 K. Note, however, that these rates can be also easily obtained for different temperatures, and this is possible due to the use of the additional calculated DFT data.

The PW91 DFT data was used earlier to derive the reaction rates used in a microkinetic model for WGSR on Cu(111) [10]. Later the same DFT data was also used to derive other set of reaction rates for a kMC study of the WGSR on a Cu/ZnO supported model catalyst [13]. In the present study, we use also these DFT data along with some extra calculations to improve more the quality of the reaction rates, specially for all endothermic reactions. However, one may

wonder whether the PW91 method is accurate enough to provide physically meaningful results in the present study. Playing the advocate devils' game one can even compare the standard change free energy (ΔG_r^o) of the WGSR in gas phase to experimental data [38], although the present study corresponds really to an open system in a nonequilibrium state. Assuming a closed system, where the WGSR achieves a thermodynamic equilibrium at a given pressure and temperature is possible to derive the equilibrium constant (K) at several temperatures. Table 2 shows some calculations carried out by means of the GAUSSIAN code [39] for ΔG_r^o and K at two temperatures (298.15 and 600 K), using different methods and a near Hartree-Fock basis set [40]. It is observed that PW91 poorly describes the thermochemistry of this reaction in gas phase at low temperature although the agreement with experiment is much better at high temperature. The results also show that the broadly used B3LYP methods designed precisely to improve the thermochemistry of reaction in gas phase [40, 41] does not perform so well, and even the golden standard CCSD(T) method exhibits some inaccuracy. At this point one can perhaps argue that results obtained for the mechanism of the WGSR reaction on the Cu(111) surface are doubtful and the doubts would have to be extended to all published articles dealing with DFT calculations of reactions taking place at metal surfaces. However, this claim is incorrect because, differently from gas phase chemistry, when the reaction takes place above a metal surface the electrons in the reacting spaces are largely screened by the electrons in the conduction band and, in addition, constitute a fraction of the total number of electrons. In this situation, PW91 and related GGA type functionals provide a very good description of the properties of the metals [42, 43, 44], where hybrid approaches, working well to describe the thermochemistry in gas phase, fail [45, 46] because of the failure to attain the exact homogeneous electron gas limit [47]. This view is supported by the large body of literature comparing DFT calculations at the GGA level (e.g., PBE or PW91) with experimental values for adsorption and reaction energies [48, 49], and is reinforced by the evidence that for reactions catalyzed by (non-magnetic) metals the transition states do not evidence any spin polarization [50]. Therefore, even if calculated results for reaction rates and related properties calculated here are by no means exact, it is very likely that the overall physical description is correct. This also supported by the excellent agreement between theory and experiment in the landmark paper of Gokhale et al. [10] reporting a microkinetic model precisely for the WGSR reaction on Cu(111).

3. Results and discussion

In this study, the effect of diffusion rates, the temperature and the reactants partial pressures on the WGSR on Cu(111) have been investigated in detail. Each kMC simulation was allowed to achieve a steady-state (typically reached between 70 and 200 million kMC steps) in which surface coverage for all intermediates reached constant values, with the exception of small fluctuations resulting from the stochastic nature of the simulation. From that point, the overall macroscopic kinetic values, such as the TOF, were calculated. For T = 625 K the total reaction rate (r_{tot}) was somewhere between 10^9 and 10^{12} s^{-1}, which means that each kMC step takes place in the sub-nanosecond time scale.

3.1 Scaled diffusion rates

Even if the diffusion processes are not rate-limiting steps in WGSR reaction, it is necessary to include them into the reaction mechanism to reach a realistic description including all possible elementary steps [20]. In the system studied here, diffusion processes have energy barriers substantially lower than those corresponding to other elementary chemical reactions (see Table 1). Consequently, most kMC steps correspond to diffusion with a small number of steps corresponding to other chemical reactions. This implies that very large simulations are required to obtain meaningful results. Using a scaling factor as shown in eq. 10 can significantly increase the efficiency of kMC simulation without affecting the results [51]. Nevertheless, it is important to appropriately choose the scaling factor which requires a few additional simulations, an effort largely compensated by the gain in speeding up the overall study. Fig. 1 reports the change of the TOF with respect to the scaling factor, and shows that selecting $\alpha=10^{-2}$, which reduces the diffusion rates by two orders of magnitude, speeds up the simulation considerably but producing almost the same TOF value as for $\alpha = 1$. A similar optimum value was taken as scaling factor in a previous kMC study of the WGSR on a model of the Cu/ZnO $(000\bar{1})$ catalyst surface [13] containing 0.2 ML Cu coverage. Thus, all simulations in the present work have been carried out by selecting $\alpha=10^{-2}$.

3.2 Temperature effects

The effect of temperature on the WGSR catalysed by Cu(111) has been investigated within the temperature range 463-625 K, where some experimental data are available for Cu(111) single-crystal catalyst [52] and $CuO/ZnO/Al_2O_3$ catalysts [5, 53]. Most of the theoretical studies of the WGSR on Cu surfaces are also within this temperature range [10,11,13, 23]. We observe that raising the temperature within this range increases the value of the reaction rates and hence one would expect an increase of the TOF too. However, the overall kinetics is controlled not only by the reaction rates, but also by the surface coverage of the different species. Plotting the logarithm of the simulated TOF as function of 1000/T leads to an Arrhenius behaviour (see Fig. 2) in two temperature intervals, with apparent activation energies of 0.5 eV (525-625 K) and 0.8 eV (463-525 K). A very similar behaviour was observed for WGSR on Pt(111) (see supplementary material on Ref. 23). The experimental value reported of the apparent activation energy of WGSR on a clean Cu(111) single-crystal surface with 10 Torr (1.33 mbar) H_2O and 26 Torr (34.7 mbar) CO was 0.7 eV at 563–683 K [52], which is very close to the present calculated values; other reported values of the apparent activation energies of Cu-based catalysts fall within the interval 0.7±0.2 eV [5, 53], supporting that the metallic Cu seems to be the active phase for WGSR. A more recent kinetic study for WGSR at 1 atm of total pressure and a temperature close to 463 K [5] reports an apparent activation energy of 0.8 eV for a Cu-based catalyst (i.e., $CuO/ZnO/Al_2O_3$), in excellent agreement also with the present kMC calculated value. However, it is important to point out that a direct comparison with the apparent activation energies reported in the literature is rather complicated by the fact that most studies were carried out under different conditions. For instance, CO_2 and H_2 were also included into the reactants mixture to study their inhibitory effects (i.e., negative reaction orders, see Table 4 in Ref. 5) whereas in the present study these products leave the surface region.

Fig. 3 shows the statistics of the most important elementary processes at T = 463 K (left) and 625 K (right), showing the number of events per site and per time unit for the forward and reverse processes. At low temperatures, the system spends a considerable amount of time just in adsorption and desorption processes of both reactants. When water molecules start to dissociate according to process +5 (see Table 1), OH adsorbed species become available on the surface and processes +7 and -7 begin to occur. If a CO molecule is adsorbed besides an OH, it immediately

oxidizes CO to form the *cis*-carboxyl intermediate, changing then to the more stable *trans* conformation (i.e., processes +9 and +10) until it finds another OH to form CO_2 through an associative route (i.e., processes +12). Thus, the reaction is mainly controlled by processes +5 and +12.

At higher temperatures (625 K) the system also spends some time with adsorption/desorption of both reactants, but the frequency of water dissociation is much higher, lowering the surface coverage of water and greatly increasing the number of adsorbed OH intermediates (see Fig. 4). Thus, processes +7 and -7 occur with a much higher frequency (see Fig. 3, right). In addition, processes -5, -9 and -12 also increase significantly their frequencies. Therefore, in these conditions the processes +10 and +12 seem to control the reaction. The observed change in the rate-limiting steps with the temperature increment may be related with the decrease of the apparent activation energy shown in Fig. 2.

It is important to mention that, despite the high number of elementary processes, the stoichiometry of the global reaction is preserved, except for the first simulation steps, where the $CO_{2(g)}$ production is faster than the $H_{2(g)}$ production. Interestingly enough, this fact is also experimentally observed [52]. The present kMC simulations also confirm that the associative mechanism mediated by carboxyl (COOH) intermediate provides the dominant reaction path, and that the redox or the formate mediated mechanisms do not play a significant role, in agreement with previous microkinetic models [10, 54, 55]. The same conclusion was found in the theoretical study of Tang and He [11]. However, on the WGSR catalysed by Cu nanoparticles supported on a ZnO surface, where two types of active sites (edges and (111) terraces) were used to model Cu nanoparticles, both redox and COOH-mediated mechanisms are competing, because edge sites favours the former [13].

An important piece of information coming out from the kMC simulations can be obtained from inspection of the average surface coverage for the main species, which are plotted in Fig. 4. First, note that carboxyl species are very reactive and its coverage is almost insignificant. From this plot one can also clearly see that H_2O and H are the dominant species at low temperatures, occupying an important part of surface sites (i.e., 72% at 463 K) whereas OH and H are dominant at high temperatures but with a lower total coverage (i.e., 44% at 625 K); the higher the reaction temperature, the lower the total coverage. As shown in this figure, CO lateral

interactions will not play an important role in the WGSR due to the negligible CO coverage at the final steady-state.

Unfortunately, calculated surface coverage values are very difficult to compare with results in the literature, mainly because they are very different depending on the experimental working conditions such as pressure, temperature or catalysts employed. A similar situation occurs for previous theoretical studies where surface coverage values depend on the model and methodology used. Thus, a previous microkinetic model of the WGSR on Cu(111) [56] predicts that under most reaction conditions surface coverage by reaction intermediates is small, although water is found to be the most abundant species on the surface for low H_2O/CO ratios. Another microkinetic model [55] confirms this small coverage, finding also H_2O, CO and H as the main species, with H_2O and CO coverage decreasing and H coverage slightly increasing when temperature is augmented. Nevertheless, the more recent microkinetic model from Mavrikakis et al. [10] for WGSR on Cu(111) shows that at high pressures (1-20 bar) bidentate formate and atomic H are the most abundant surface species, whereas CO and H_2O coverage are very low. In other kMC study of the WGSR on Pt(111) [51] it was observed that CO coverage was dominant (~70-80 % for 650 K P_{H2O} = 0.1 bar and P_{CO} = 0.05 bar) while water coverage was very low, a behaviour quite different from that corresponding to the WGSR on Cu(111), either from experimental or from theoretical simulations.

In the present study, we observe high water coverage at the lowest temperature studied (i.e., 0.43 at 463 K, Fig. 4), which becomes very low at the highest temperature (i.e., $1 \cdot 10^{-2}$ at 625 K, Fig. 4). This latter value compares quite well with the low experimental value for H_2O coverage at 612 K (i.e., $5 \cdot 10^{-4}$ [52]), which should be taken rather qualitatively because includes several assumptions and parameters for the Cu(110) surface. The reason for the high water coverage at 463 K can be understood by analysing the water adsorption/desorption rates. At low temperature the adsorption reaction rate is almost twice larger that than for desorption, leading to a higher final water coverage, whereas at high temperatures the desorption reaction rate is two orders of magnitude larger than that for adsorption and thus the water coverage is very low as could be expected.

One of the aspects that makes kMC method such a powerful tool is that one can obtain information regarding the structure of the adlayer at any moment of the simulation. Fig. 5 shows

snapshots of the Cu(111) surface at the beginning of the simulation (left) and once the steady-state (SS) is reached (right), at 463 K (top) and 625 K (bottom) for a given reactants mixture (P_{H2O} = 10 Torr and P_{CO} = 26 Torr). The time to reach the SS depends heavily on the temperature: at 463 K the SS is typically reached after 2 ms (about 70 million kMC steps), whereas at 625 K it takes 60 μs (about 200 million kMC steps). Although the total time needed to reach the SS is lower when the temperature is increased, longer simulations are required because the number of kMC steps is increased too. These snapshots apart from confirming the main adsorbed species implied in the SS (Fig. 4), also show that the assumption from macroscopic rate equations that the adsorbates are randomly distributed is not always correct. At low temperatures (Fig. 5b) there is a correlation in the occupation of neighbouring sites, and at very low temperatures may even result in island formation of ordered adlayers [20]. However, this correlation seems to be negligible at higher temperatures (Fig. 5d).

In order to see if the formation of H/H_2O islands, as no adsorbate interactions were included in the kMC simulations, could be perhaps related with the inclusion of a scaling factor for diffusion derived for higher temperatures, we carried out additional simulations at 463 K, concluding than selecting $\alpha = 0.01$ still produces almost the same TOF than for $\alpha = 1$ (i.e., $10^{2.16}$ and $10^{2.15}$ for $\alpha = 0.01$ and 1, respectively). Thus, the formation of H/H_2O islands was not a result of the use of an unreliable scaling factor. In fact, this behaviour can be explained as a consequence of a correlation due to the reactions (see Ref. 20, pg. 2-3): at 463 K the water coverage at the initial steps of the simulation is very high (Fig. 5a); when water molecules dissociate, they generate OH+H pairs, and H_2O/OH/H islands start growing. Adsorbed CO molecules rapidly consume the adsorbed OHs (i.e., leading to a low OH coverage) forming COOHs, which in turn react rapidly with other OHs to form more water and CO_2 (that rapidly desorb) and the cycle is repeated. So, at the end what remains are the H/H_2O islands observed in Fig. 5b. Moreover, surface H atoms are accumulated due to the low reaction rate for H_2 formation at 463 K (i.e., $2.8 \cdot 10^2$ s^{-1}) compared with the other processes. At 625 K this reaction rate is much higher ($1.5 \cdot 10^5$ s^{-1} in Table 1) and those H-islands are almost not observed (Fig. 5d).

3.3 Partial pressure effects

The effect of reactants mixture composition on the overall H_2 production has been examined carrying out simulations by varying the partial pressure of one of the reactants from 1 to 25 Torr while keeping constant the partial pressure of the other reactant (i.e., fixing 26 Torr for CO or 10 Torr for H_2O). The results summarized in Fig. 6 indicate that at low total pressures the partial orders for CO and H_2O are 0.7 and 0.6, respectively. For a similar pressure range and temperature (612 K) for the WGSR on Cu(111), Campbell et al. [52] found a partial order in water between 0.5-1, in agreement with the present result, but surprisingly they reported a zero value for the partial order in CO. However, usually positive and similar partial orders of both reactants have been found in other previous microkinetic models of the WGSR on Cu(111) (e.g., 0.90 and 0.85 for 1 bar of total pressure [10], 0-0.8 and 0.8-1 depending on temperature for total pressures until 30 bar [54], ~0 and 0.9-1 depending on temperature for a total pressure of 1.5 atm [55], for CO and H_2O, respectively) and in several experiments (e.g., 0.8 and 0.8 for 1 atm of total pressure and a temperature close to 463 K [5], 1 (assumed) and 1.4 for 5 bar of total pressure and a temperature close to 463 K [55], for CO and H_2O, respectively). Since both calculated reaction orders are lower than 1, TOF converges to a constant value for very high pressures of CO and H_2O, limited by the available number of free sites in the catalyst and maybe by the repulsive lateral interactions between CO adsorbates.

The H_2O/CO ratio in the initial reactants mixture plays a very important role in the WGSR. Thus, a series of kMC simulations were performed at H_2O/CO ratios ranging from 0.1 to 9.0 for a total pressure of 100 Torr and for a temperature of 625 K (Fig. 7). It can be seen that TOF passes through a maximum around a H_2O/CO ratio of 0.43-0.66, close to the experimental selected conditions (i.e., 0.38 for 10 Torr H_2O and 26 Torr CO in [52]). This need for a higher pressure of CO can be explained using the information of the reaction rates (Table 1); at 625K the rate for CO desorption is two orders of magnitude larger than for water, therefore a higher pressure of CO should be used to compensate its larger desorption. This result is also in agreement with the slightly higher reaction order found for CO compared to H_2O at the low total pressures used in Fig. 6.

There is a clear relationship between TOF and H coverage as can be seen from Fig. 7. The larger the amount of H adsorbed at the surface, the higher the probability to form molecular hydrogen via process -2 ; this is also true for CO_2 formation. For all of these initial conditions the

stoichiometry of the WGSR is perfectly maintained, except in the initial steps of the simulations with high H_2O/CO ratios, where hydrogen is firstly produced with a high TOF and then its rate decays slowly until a lower value at the same instant at which begins the production of CO_2.

Finally, it is also observed that as the H_2O/CO initial ratio increases the concentration of adsorbed OH increases. This effect was also observed in the rather old kinetic model of Ovesen et al. [56]. For very high H_2O/CO ratios, the TOF of the reaction would drop rapidly because of OH poisoning of the surface. Likewise, in a more recent study [57] it was found that copper catalysts retain their high activity and selectivity for the WGSR when the reactants' feeding operates a low H_2O/CO ratio at low temperatures.

We have also made a study of the increase of the total pressure on the WGSR. Thus, we have considered 1 bar of pressure ($P_{CO}=P_{H2O}$=375 Torr = 0.5 bar) and a temperature of 625K. In these conditions TOF was $7.1 \cdot 10^4$ s^{-1}, larger than the value obtained for lower pressure ($P_{CO}=P_{H2O}$= 10 Torr) and the same H_2O/CO ratio (TOF = $5.2 \cdot 10^3$ s^{-1}) as could be expected because reactants pressure/concentration increases; larger coverages for H and H_2O were also obtained, and a small presence of adsorbed formate was observated. Probably, formate formation could be more enhanced when working with partial pressures of CO_2 and H_2 different from zero (i.e., products participating in the initial reactants mixture); in this case, processes +15 and +16 (see table 1), although with low reaction rates, would be more important due to the major presence of CO_2* and would explain formate formation.

4. Conclusions

In this work, we present a first-principles based kMC simulation of the water gas shift reaction on Cu(111) surface including a total of 34 elementary processes, such as adsorption/desorption, diffusion and other elementary surface chemical reactions. Reactions rates were obtained by application of both transition state theory or collision theory, with also an inclusion of one-dimensional tunnelling correction for reactions involving hydrogen atom transfer. Diffusion reaction rates were scaled enough to accelerate those simulations without affecting the final results. Earlier density functional theory results along with additional calculations were used for the computation of reaction rates at several temperatures.

The effect of temperature on WGSR was studied in the 463-625 K range, showing an Arrhenius behaviour with an activation energy of 0.8 eV at lower temperatures and a smaller value of 0.5 eV for higher ones. This behaviour can explained due to the change in the rate-limiting step from low (water dissociation) to high (carboxyl isomerization) temperature. In both cases the associative mechanism mediated by carboxyl (COOH) intermediate provides the dominant reaction path, and the redox or the formate mediated mechanisms do not play a significant role.

Surface coverage was also analysed, indicating that H_2O and H are the main adsorbed species at low temperatures whereas OH and H are the dominant at high temperatures.

The effect of reactants initial mixture composition (i.e., H_2O/CO ratio) was also studied, observing that mixtures with higher CO proportion enhance the production of H_2 in the WGSR.

In spite of the present simulations have been carried out for the Cu(111) surface, which in principle could be assumed as an ideal catalyst, previous studies confirm that the metallic Cu seems to be the active phase for WGSR catalysed with different Cu-based catalysts. However, further kMC studies with Cu-stepped surfaces are in progress to ascertain the effect of possible lower energy barriers in some of the elementary steps (e.g., for water dissociation) and its influence into the final WGSR mechanism and TOF, which will allow to give more chemical insights to design more efficient catalysts.

We further demonstrated the capabilities of the kMC method to model complex surface reactions, providing a large amount of information, like apparent activation energies, surface coverage as function of temperature or reactants partial pressure, optimum reactants mixture composition, and the structure of the adlayer at atomic scale, among other data, which can not be obtained all together from previous theoretical approaches or experiments.

Acknowledgments

The authors are indebted to Prof. Manos Mavrikakis for sending unpublished DFT data from Ref. 10 and for useful comments. The authors acknowledge support from the Spanish MINECO CTQ2012-30751 and CTQ2014-53987-R grants and, in part, from the Generalitat de Catalunya grants 2014SGR97, 2014SGR1582 and XRQTC. Leny Álvarez is grateful to the

Secretaría de Ciencia y Tecnología e Innovación del Distrito Federal de la Ciudad de México for the financial support to her postdoctoral research at the Institute of Theoretical and Computational Chemistry of *Universitat de Barcelona* (IQTC-UB).

Table 1. Energy barriers (E_b in eV) and reaction rates (r_i in s^{-1}) for all the elementary processes included in the simulation (T = 625K, P_{CO} = 26 Torr, P_{H2O} = 10 Torr). Energy barriers with zero point energy correction from: a) Ref. 10, b) Ref. 13 and c) Ref. 10 along with additional present DFT calculations.

		Forward		Reverse	
ID	Elementary process	E_b	r_i	E_b	r_i
1	CO (g)↔CO*	0.00[a]	4.00×10^{6}	0.51[a]	1.02×10^{10}
2	H_2 (g)←2H*	-	-	0.96[a]	1.51×10^{5}
3	H_2O (g)↔H_2O*	0.00[a]	1.92×10^{6}	0.18[a]	1.08×10^{8}
4	CO_2 (g) ← CO_2*	-	-	0.09[a]	1.67×10^{8}
5	H_2O* ↔ OH* + H*	1.01[c]	4.55×10^{5}	1.15[a]	1.18×10^{4}
6	OH* ↔ O* + H*	1.60[c]	2.30×10^{0}	1.19[a]	3.17×10^{3}
7	2OH* ↔ H_2O* + O*	0.68[c]	1.86×10^{8}	0.00[a]	2.75×10^{13}
8	CO* + O* ↔ CO_2*	0.79[a]	8.07×10^{6}	1.57[c]	4.88×10^{0}
9	CO* + OH* ↔ *cis*-COOH*	0.70[c]	4.99×10^{7}	0.55[a]	3.38×10^{8}
10	*cis*-COOH* ↔ *trans*-COOH*	0.48[a]	1.23×10^{9}	0.70[c]	2.65×10^{7}
11	*trans*-COOH* ↔ CO_2* + H*	1.18[a]	5.57×10^{3}	1.69[c]	3.19×10^{-1}
12	*trans*-COOH* + OH* ↔ CO_2* + H_2O*	0.38[a]	1.31×10^{10}	0.75[c]	1.45×10^{7}
13	CO_2*+ H* ↔ HCOO*	1.00[c]	1.05×10^{5}	0.54[a]	8.44×10^{8}
14	HCOO* ↔ HCOO**	0.04[a]	6.11×10^{12}	0.48[c]	1.82×10^{9}
15	CO_2* + H_2O* ↔ HCOO** + OH*	1.61[a]	1.18×10^{0}	1.71[c]	2.12×10^{-1}
16	CO_2* + OH* ↔ HCOO** + O*	2.09[c]	1.84×10^{-4}	1.71[a]	2.38×10^{-1}
17	CO* + * → * + CO*	0.08[b]	2.18×10^{10}	0.08[b]	2.18×10^{10}
18	OH* + * → * + OH*	0.12[b]	1.06×10^{10}	0.12[b]	1.06×10^{10}
19	H* + * → * + H*	0.15[b]	6.77×10^{9}	0.15[b]	6.77×10^{9}
20	O* + * → * + O*	0.38[b]	8.31×10^{7}	0.38[b]	8.31×10^{7}

Reaction rates were calculated using TST equations excepting for processes 1 and 3, where collision theory and detailed balance principle were used.
The optimum scaling factor α for diffusion processes (17-20) was taken to be 0.01.

Table 2. Calculated standard change of free energy (kcal/mol) of the WGSR at 298.15 K and 600 K with different DFT functionals and with the post-HF CCSD(T) method, using the aug-cc-pVTZ basis set, compared with the experimental value Ref. 38. Equilibrium constant ($\Delta G_r^o = -RTlnK$) is also reported for comparison.

	$\Delta G^o_{r,298}$	$\Delta G^o_{r,600}$	K_{298}	K_{600}
PBE	-17.36	-14.52	5.3×10^{12}	1.9×10^{5}
PW91	-16.99	-9.98	2.8×10^{12}	4.0×10^{3}
B3LYP	-11.51	-8.64	2.7×10^{8}	1.4×10^{3}
CCSD(T)	-5.56	-2.69	1.2×10^{4}	9.6
Exp.	-6.85	-3.99	1.0×10^{5}	28

Fig. 1. H_2 productivity as a function of the scaling α factor. Simulations performed at T = 625 K, P_{CO} = 26 Torr and P_{H2O} = 10 Torr

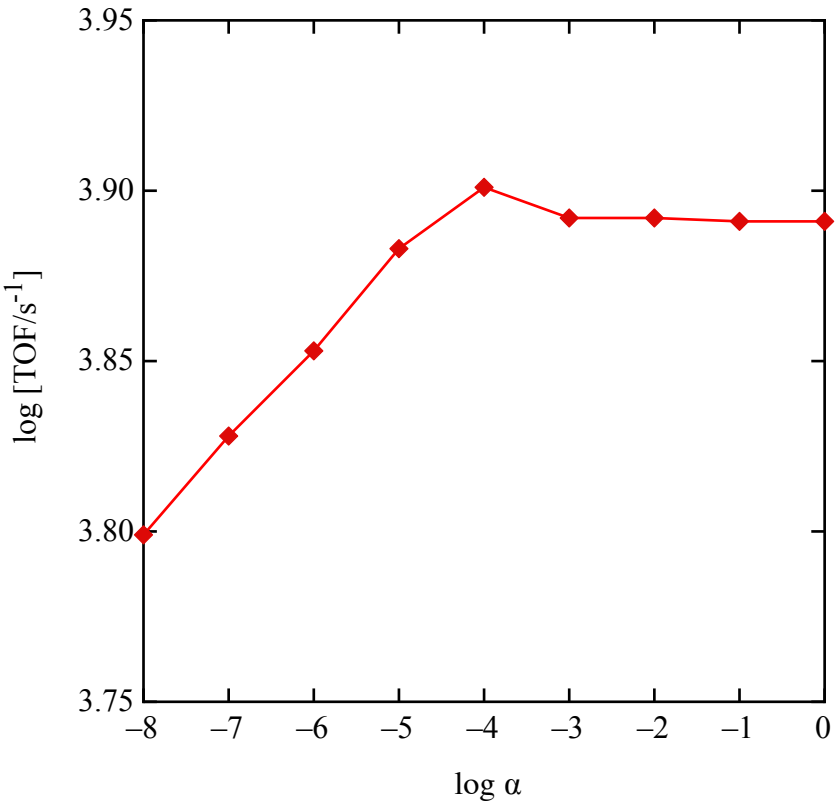

Fig. 2. Arrhenius plot of the WGSR TOF in the temperature range 460-625 K. Simulations performed at P_{CO} = 26 Torr and P_{H2O} = 10 Torr.

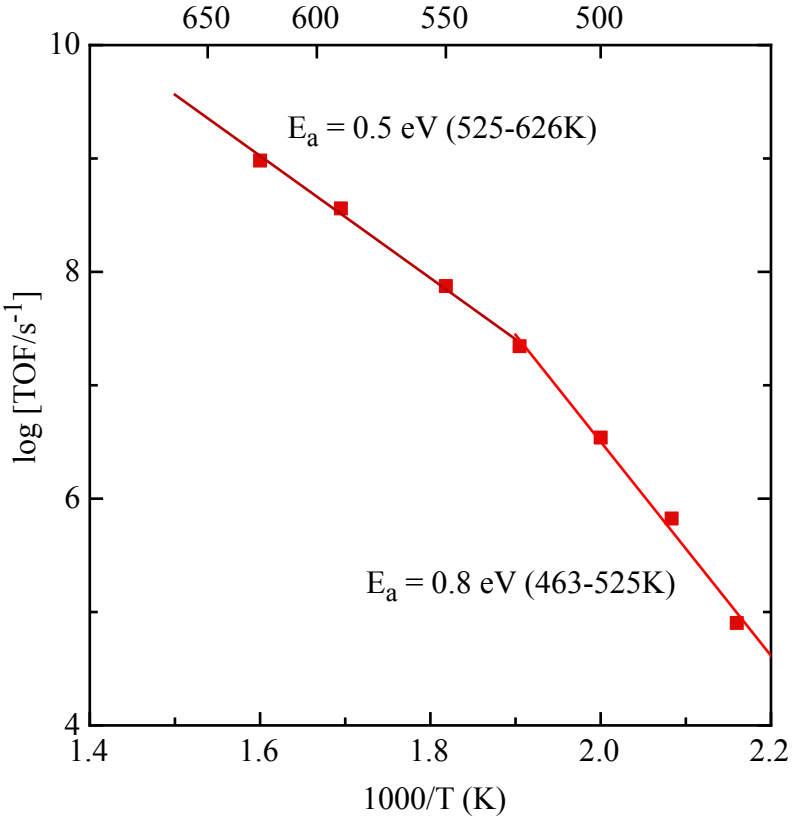

Fig. 3. Main elementary processes (direct in red and reverse in blue) and their frequencies for the WGSR at Cu(111) at P_{CO} = 26 Torr, P_{H2O} = 10 Torr and T = 463 K (left) and 625 K (right).

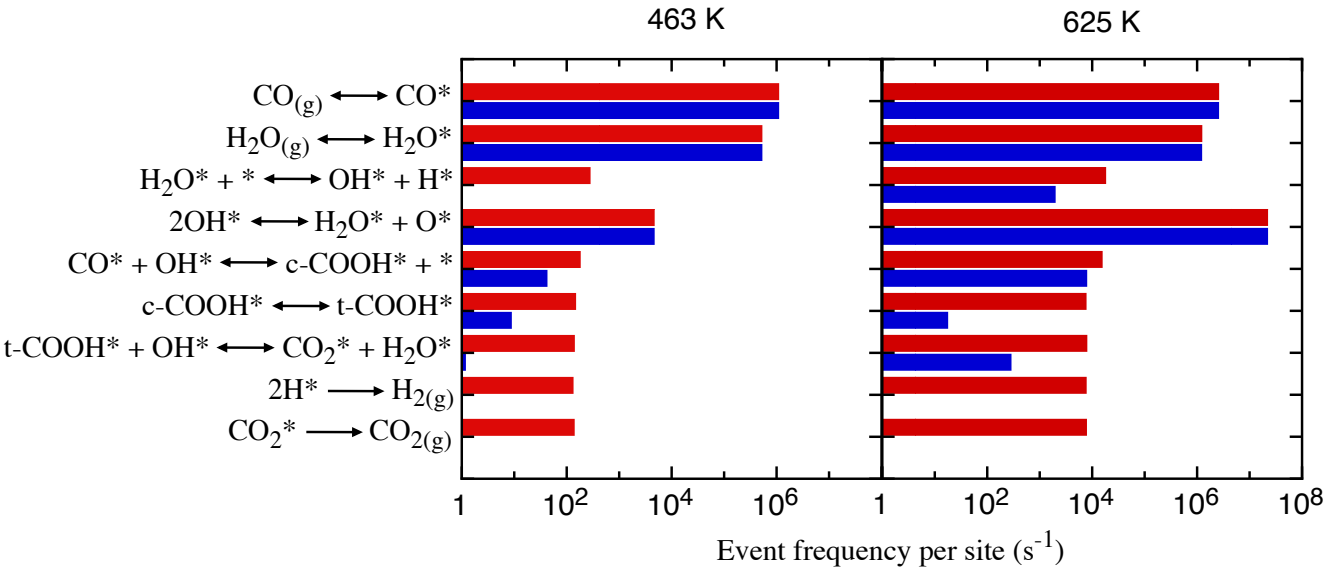

Fig. 4. Surface coverage of several species as a function of temperature for P_{CO} = 26 Torr and P_{H2O} = 10 Torr.

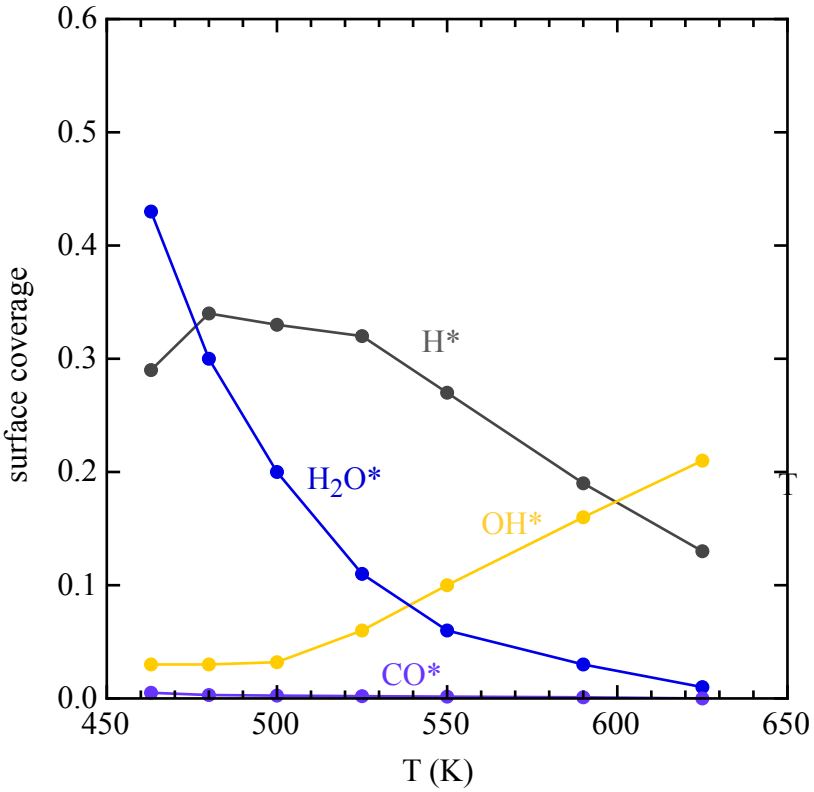

Fig. 5. Snapshots of the surface coverage at the beginning and once achieved the stead-state at two temperatures and P_{H2O} = 10 Torr and P_{CO} = 26 Torr. Surface Cu atoms are shown in white colour.

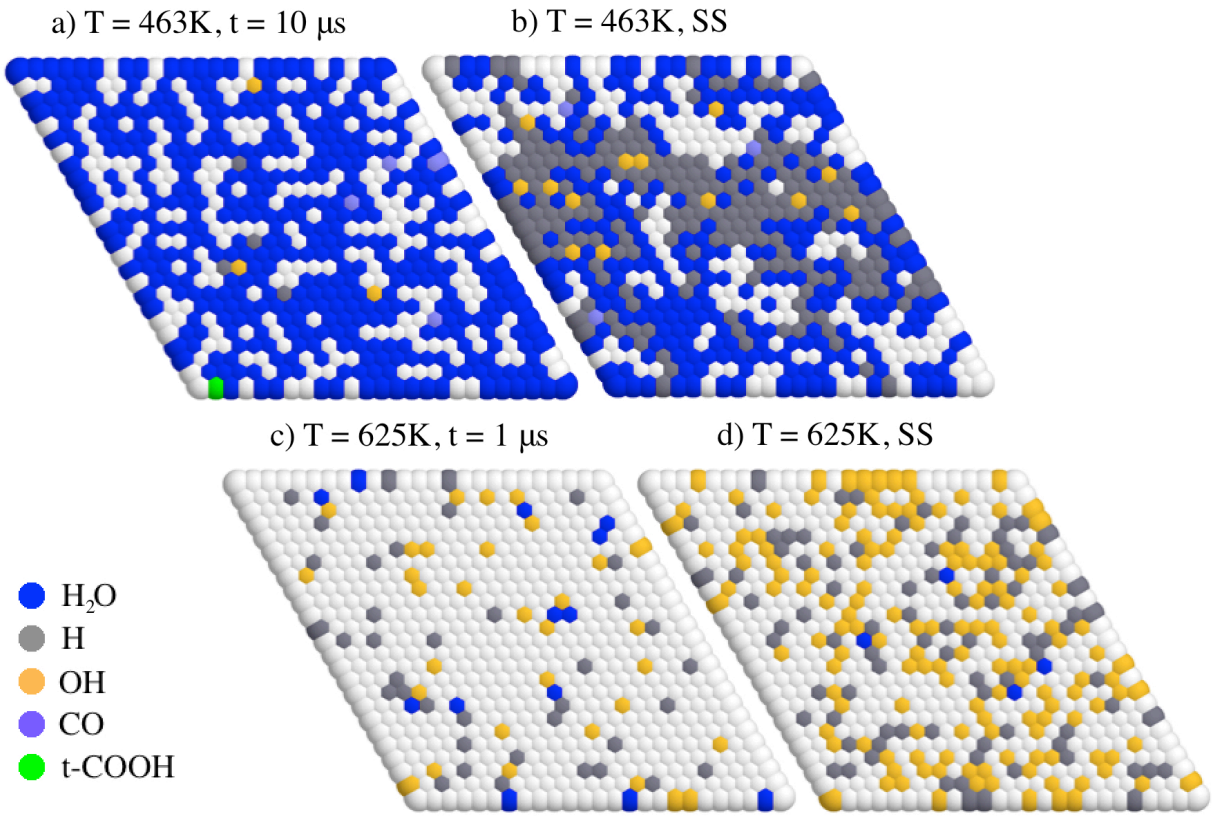

Fig. 6. H_2 formation at T = 625 K as a function of reactants partial pressures. Red line (circles) corresponds to the variation of P_{CO} when P_{H2O} = 10 Torr and blue line (squares) corresponds to the variation of P_{H2O} when P_{CO} = 26 Torr.

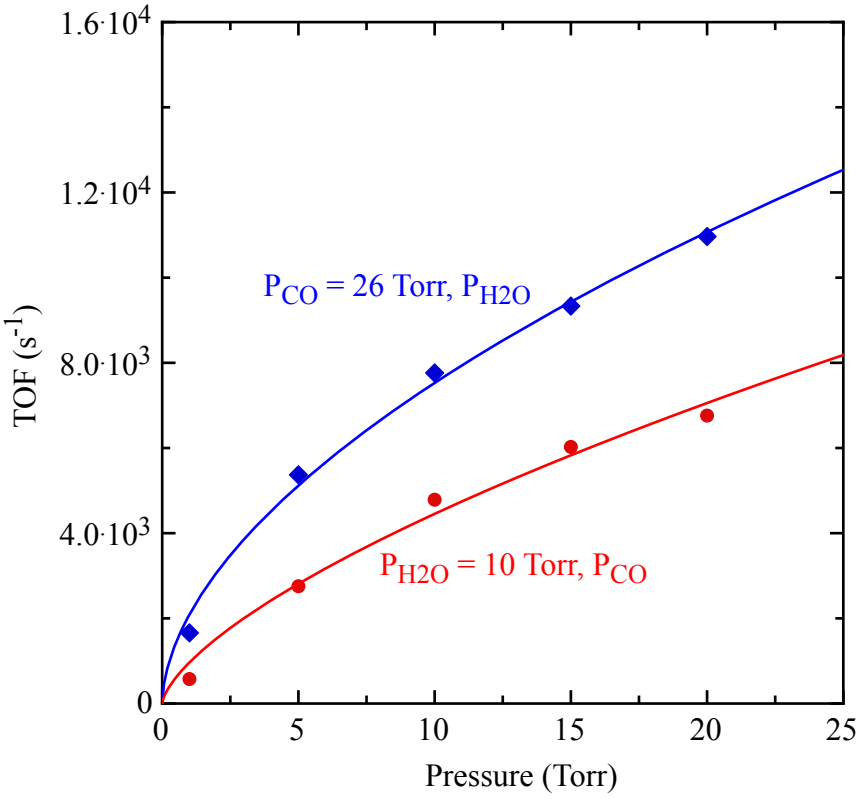

Fig. 7. Surface coverage of several species (coloured lines) and TOF based on $H_{2(g)}$ formation (black line) as a function of the partial pressures of reactants for a total pressure of 100 Torr. Simulations performed at T = 625K.

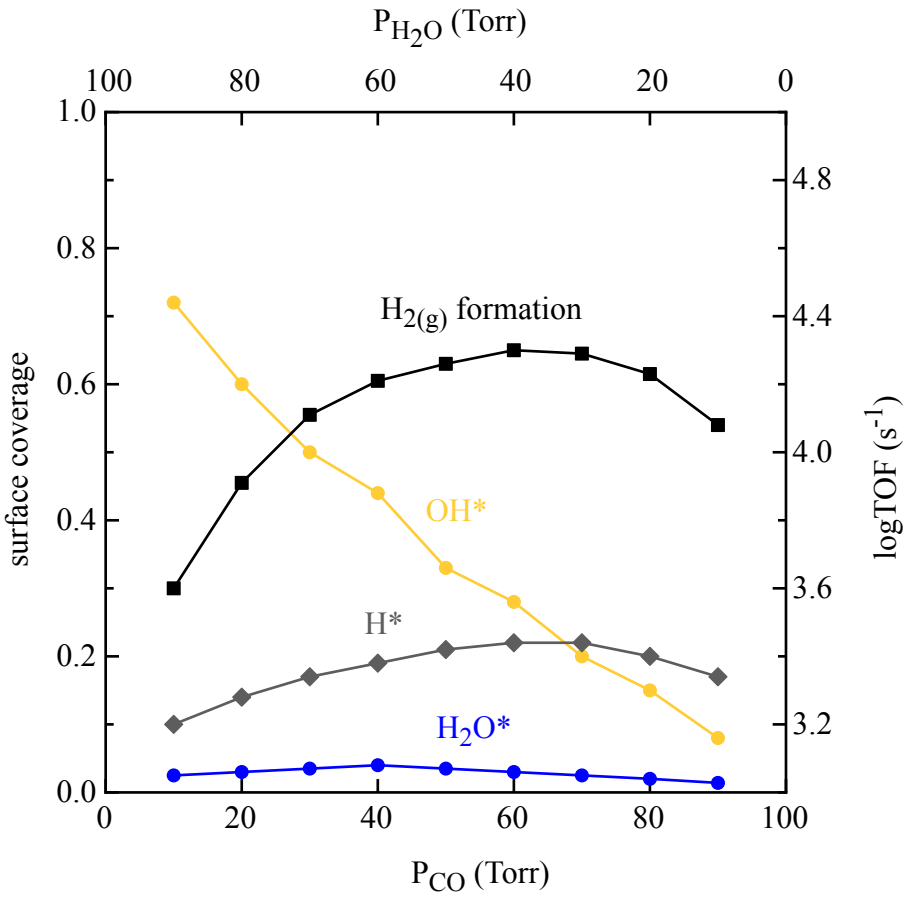

References

[1] M. Flytzani-Stephanopoulos, Gold atoms stabilized on various supports catalyze the water–gas shift reaction, Acc. Chem. Res. 47 (2014) 783-792.

[2] J.R. Ladebeck, J.P. Wagner, in: Handbook of Fuel Cells: Fundamentals, Technology and Applications; W. Vielstich, A. Lamm , A.H. Gasteiger, Ed., John Wiley & Sons, Chichester, UK, 2003, vol 3, p. 190-201.

[3] D.S. Newsome, The water-gas shift reaction, Catal. Rev. Sci. Eng. 21 (1980) 275-318.

[4] D.W. Jeong, W.J. Jang, J.O. Shim, W.B. Han, H.S. Roh, U.H. Jung, W.L. Yoon, Low-temperature water-gas shift reaction over supported Cu catalysts, Renew. Energ. 65 (2014) 102-107.

[5] N.A. Koryabkina, A.A. Phatak, W.F. Ruettinger, R.J. Farrauto, F.H. Ribeiro, Determination of kinetic parameters for the water-gas shift reaction on copper catalysts under realistic conditions for fuel cell applications, J. Catal. 217 (2003) 233-239.

[6] D. Falleiros, F. Ademar, M. Kaminski, P. Matar, in: Petrochemicals, V. Patel, Ed., Intech, Rijeka, Croatia, 2012, chap. 4.

[7] J.P. Clay, J.P. Greely, F.H. Ribeiro, W.N. Delgass, W.F. Schneider, DFT comparison of intrinsic WGS kinetics over Pd and Pt, J. Catal. 320 (2014) 106-117.

[8] M. Stamatakis, Y. Chen, G. Vlachos, First-principles-based kinetic Monte Carlo simulation of the structure sensitivity of the water-gas shift reaction on platinum surfaces, J. Phys. Chem. C 115 (2011) 24750-24762.

[9] J.L.C. Fajín, M.N.D.S. Cordeiro, F. Illas, J.R.B. Gomes, Influence of step sites in the molecular mechanism of the water gas shift reaction catalysed by copper, J. Catal. 268 (2009) 131-141.

[10] A.A. Gokhale, A.J. Dumesic, M. Mavrikakis, On the mechanism of low-temperature water gas shift reaction on copper, J. Am. Chem. Soc. 130 (2008) 1402-1414.

[11] Q. Tang, Z. Chen, X. He, A theoretical study of the water-gas shift reaction mechanism on Cu(111) model system, Surf. Sci. 603 (2009) 2138-2144.

[12] K. Mudiyanselage, S.D. Senanayake, L. Feria, S. Kundu, A.E. Baber, J. Graciani, A.B. Vidal, S. Agnoli, J. Evans, R. Chang, S. Axnanda, Z. Liu, J.F. Sanz, P. Liu, J.A. Rodriguez, D.J. Stacchiola, Importance of the metal-oxide interface in catalysis: in situ studies of the water-gas

shift reaction by ambient-pressure X-ray photoelectron spectroscopy, Ang. Chem. 125 (2013) 5205-5209.

[13] L. Yang, A. Karim, J.T. Muckerman, Density functional kinetic Monte Carlo simulation of water-gas shift reaction on Cu/ZnO, J. Phys. Chem. C 117 (2013) 3414-3425.

[14] J.A. Rodriguez, J. Evans, J. Graciani, J.B. Park, J. Hrbek, J.F. Sanz, High water-gas shift activity in TiO_2(110) supported Cu and Au nanoparticles: role of the oxide and metal particle size, J. Phys. Chem. C 113 (2009) 7364-7370.

[15] J.A. Rodriguez, PJ. Ramírez, G.G. Asara, F. Viñes, J. Evans, P. Liu, J.M. Ricart, F. Illas, Charge polarization at a Au-TiC interface and the generation of highly active and selective catalysts for the low-temperature water-gas shift reaction, Angew. Chem. Int. Ed. 53 (2014) 11270-11274.

[16] F. Tao, Z. Ma, Water-gas shift on gold catalysts: catalyst systems and fundamental studies, Phys. Chem. Chem. Phys. 15 (2013) 15260-15270.

[17] J.B. Park, J. Graciani, J. Evans, D. Stacchiola, S.D. Senanayake, L. Barrio, P. Liu, J.F. Sanz, J. Hrbek, J.A. Rodriguez, Gold, copper, and platinum nanoparticles dispersed on CeO_X/TiO_2(110) surfaces: high water-gas shift activity and the nature of the mixed-metal oxide at the nanometer level, J. Am. Chem. Soc. 132 (2010) 356-363.

[18] J. Graciani, J.F. Sanz, Designing a new generation of catalysts: water gas shift reaction example, Catal. Today. 240 (2014) 214-219.

[19] R.A. Hadden, P.D. Lambert, C. Ranson, Relationship between the copper surface area and the activity of $CuO/ZnO/Al_2O_3$ water-gas shift catalysts, App. Cat. A: Gen. 122 (1995) L1-L4.

[20] A.P.J. Jansen, An introduction to kinetic Monte Carlo simulations of surface reactions, Lecture Notes in Physics, vol. 856, Springer-Verlag, Heidelberg, Germany, 2012.

[21] A. Chatterjee, D.G. Vlachos, An overview of spatial microscopic and accelerated kinetic Monte Carlo methods, J. Comput. Aided Mater. Des. 14 (2007) 253-308.

[22] K. Reuter, in: Modeling and simulation of heterogeneous catalytic reactions, O. Deutschmann, Ed., Wiley-VCH Verlag GmbH and Co. KGaA, Weinheim, Germany, 2011, p. 71-111.

[23] M. Stamatakis, D.G. Vlachos, A graph-theoretical kinetic Monte Carlo framework for on-lattice chemical kinetics, J. Chem. Phys. 134 (2011) 214115.

[24] J. Nielsen, M. d'Avezac, J. Hetherington, M. Stamatakis, Parallel kinetic Monte Carlo simulation framework incorporating accurate models of adsorbate lateral interactions, J. Chem. Phys. 139 (2013) 224706.

[25] K.J. Laidler, Chemical kinetics, Harper & Row Publishers, New York, USA, 1987.

[26] I. Bönicke, W. Kirstein, S. Spinzig, F. Thieme, CO adsorption studies on a stepped Cu(111) surface, Surf. Sci. 313 (1994) 231-238.

[27] B.J. Hinch, L.H. Dubois, Chem. Water adsorption on Cu(111): evidence for Volmer-Weber film growth, Phys. Lett. 181 (1991) 10-15.

[28] CRC Handbook of Chemistry and Physics, 88th ed., D.R. Lide, Ed., CRC Press, Boca Raton, USA, 2008.

[29] K. Reuter, M. Scheffler, First-principles kinetic Monte Carlo simulations for heterogeneous catalysis: application to the CO oxidation at RuO_2(110), Phys. Rev. B 73 (2006) 045433.

[30] J.I. Steinfeld, J.S. Francisco, W.L. Hase, Chemical kinetics and dynamics, Prentice Hall, Englewood Cliffs, USA, 1989.

[31] G. Kresse, J. Hafner, Ab initio molecular dynamics for liquid metals, Phys. Rev. B 47 (1993) 558 -561.

[32] G. Kresse, J. Furthmüller, Efficiency of ab-initio total energy calculations for metals and semiconductors using a plane-wave basis set, Comput. Mater. Sci. 6 (1996) 15 -50.

[33] G. Kresse, J. Furthmüller, Efficient iterative schemes for ab initio total-energy calculations using a plane-wave basis set, Phys. Rev. B 54 (1996) 11169 -11186.

[34] P.E. Blöchl, Projector augmented-wave method, Phys. Rev. B 50 (1994) 17953.

[35] G. Kresse, D. Joubert, From ultrasoft pseudopotentials to the projector augmented-wave method, Phys. Rev. B 59 (1999) 1758 -1755.

[36] H.J. Monkhorst, J.D. Pack, Special points for Brillouin-zone integrations, Phys. Rev. B 13 (1976) 5188 -5192.

[37] J.P. Perdew, J.A. Chevary, S.H. Vosko, K.A. Jackson, M.R. Pederson, D.J. Singh, C. Fiolhais, Atoms, molecules, solids, and surfaces: applications of the generalized gradient approximation for exchange and correlation, Phys. Rev. B 46 (1992) 6671 -6687.

[38] M.W. Chase Jr, NIST-JANAF thermochemical tables, J. Phys. Chem. Ref. Data Monograph 9, 4th edn. American Institute of Physics, New York, 1998.

[39] Gaussian 09, Revision D.01, M. J. Frisch, G. W. Trucks, H. B. Schlegel, G. E. Scuseria, M. A. Robb, J. R. Cheeseman, G. Scalmani, V. Barone, B. Mennucci, G. A. Petersson, H. Nakatsuji, M. Caricato, X. Li, H. P. Hratchian, A. F. Izmaylov, J. Bloino, G. Zheng, J. L. Sonnenberg, M. Hada, M. Ehara, K. Toyota, R. Fukuda, J. Hasegawa, M. Ishida, T. Nakajima, Y. Honda, O. Kitao, H. Nakai, T. Vreven, J. A. Montgomery, Jr., J. E. Peralta, F. Ogliaro, M. Bearpark, J. J. Heyd, E. Brothers, K. N. Kudin, V. N. Staroverov, R. Kobayashi, J. Normand, K. Raghavachari, A. Rendell, J. C. Burant, S. S. Iyengar, J. Tomasi, M. Cossi, N. Rega, J. M. Millam, M. Klene, J. E. Knox, J. B. Cross, V. Bakken, C. Adamo, J. Jaramillo, R. Gomperts, R. E. Stratmann, O. Yazyev, A. J. Austin, R. Cammi, C. Pomelli, J. W. Ochterski, R. L. Martin, K. Morokuma, V. G. Zakrzewski, G. A. Voth, P. Salvador, J. J. Dannenberg, S. Dapprich, A. D. Daniels, Ö. Farkas, J. B. Foresman, J. V. Ortiz, J. Cioslowski, D. J. Fox, Gaussian, Inc., Wallingford CT, 2013.

[40] A.D. Becke, Density-functional thermochemistry. III. The role of exact exchange, J. Chem. Phys. 98 (1993) 5648-5652.

[41] S. F. Sousa, P.A. Fernandes, M.J. Ramos, General performance of density functionals, J. Phys. Chem. A 111 (2007) 10439-10452.

[42] P. Janthon, S. Luo, S. M. Kozlov, F. Viñes, J. Limtrakul, D.G. Truhlar, F. Illas, Bulk properties of transition metals: A challenge for the design of universal density functionals, J. Chem. Theory Comput. 10 (2014) 3832-3839.

[43] P. Janthon, S. M. Kozlov, F. Viñes, J. Limtrakul, F. Illas, Establishing the accuracy of broadly used density functionals in describing bulk properties of transition metals J. Chem. Theory Comput. 9 (2013) 1631-1640.

[44] A. Notario-Estévez, S. M. Kozlov, F. Viñes, F. Illas, Electronic-structure-based material descriptors: (In)dependence on self-interaction and Hartree-Fock exchange, Chem. Commun. 51 (2015) 5602-5605

[45] Y. Zhao, D.G. Truhlar, Comparative assessment of density functional methods for 3d transition-metal chemistry, J. Chem. Phys. 124 (2006) 224105.

[46] N.E. Schultz, Y. Zhao, D.G. Truhlar, Density functionals for inorganometallic and organometallic chemistry, J. Phys. Chem. A 109 (2005) 11127-11143.

[47] J. Paier, M. Marsman, G. Kresse, Why does the B3LYP hybrid functional fail for metals? , J Chem Phys. 127 (2007) 024103.

[48] L. Grabow, W. Schneider, M. J. Janik, T. Manz, A. van Duin, S. Sinnott, D. Scholl, Computational Catalysis, RSC Books, A. Asthagiri (Editor), J. Spivey (Series Editor), 2013.

[49] J. K. Nørskov, F. Studt, F. Abild-Pedersen, T. Bligaard, Fundamental Concepts in Heterogeneous Catalysis, John Wiley and Sons, Hoboken, 2014.

[50] J. L. C. Fajín, M. N. D. S. Cordeiro, J. R. B. Gomes, F. Illas, On the need for spin polarization in heterogeneously catalyzed reactions on nonmagnetic metallic surfaces, J. Chem. Theory and Comput., 8 (2012) 1737-1743.

[51] M. Stamatakis, D.G. Vlachos, Equivalence of on-lattice stochastic chemical kinetics with the well-mixed chemical master equation in the limit of fast diffusion, Comput. Chem. Eng. 35 (2011) 2602-2610.

[52] T.C. Campbell, A.K. Daube, A surface science investigation of the water-gas shift reaction on Cu(111), J. Catal. 104 (1987) 109-119.

[53] C.V. Ovesen, B.S. Clausen, B.S. Hammershøi, G. Steffensen, T. Askgaard, I. Chorkendorff, J.K. Nørskov, P.B. Rasmussen, P. Stoltze, P. Taylor, A microkinetic analysis of the water-gas shift reaction under industrial conditions, J. Cat. 158 (1996) 170-180.

[54] I. Fishtik, R. Datta, A UBI-QEP microkinetic model for the water-gas shift reaction on Cu(111), Surf. Sci. 512 (2002) 229-254.

[55] C. Callaghan, I. Fishtik, R. Datta, M. Carpenter, M. Chmielewski, A. Lugo, An improved microkinetic model for the water gas shift reaction on copper, Surf. Sci. 541 (2003) 21-30.

[56] C.V. Ovesen, P. Stoltze, J.K. Nørskov, T.C. Campbell, A kinetic model of the water-gas shift reaction, J. Catal. 134 (1992) 445-468.

[57] E. Xue, M. O'Keeffe, J.R.H. Ross, Water-gas shift conversion using a feed with a low steam to carbon monoxide ratio and containing sulphur, Catal. Today 30 (1996) 107-118.

Research highlights

- A first principles kinetic Monte Carlo study of the water gas shift reaction on Cu(111).
- The associative mechanism (carboxyl intermediate) was the main reaction path.
- There is a change in the rate-limiting step from low to high temperature.
- Mixtures with higher CO proportion enhance the production of H_2.